
Article:
Li, Zhenyu and Bors, Adrian Gheorghe orcid.org/0000-0001-7838-0021 (2017) Steganalysis of 3D objects using statistics of local feature sets. Information Sciences. pp. 85-99. ISSN 0020-0255

https://doi.org/10.1016/j.ins.2017.06.011

Steganalysis of 3D Objects Using Statistics of Local Feature Sets

Zhenyu Li, Adrian G. Bors*

Department of Computer Science, University of York, York, UK YO10 5GH

Abstract

3D steganalysis aims to identify subtle invisible changes produced in graphical objects through digital watermarking or steganography. Sets of statistical representations of 3D features, extracted from both cover and stego 3D mesh objects, are used as inputs into machine learning classifiers in order to decide whether any information was hidden in the given graphical object. According to previous studies, sets of local geometry features can be used to define the differences between stego-objects and cover-objects. The features proposed in this paper include those representing the local object curvature, vertex normals, the local geometry representation in the spherical coordinate system and are considered in various combinations with others. We also analyze the effectiveness of various 3D feature sets applied for steganalysis based on the Pearson correlation coefficient. Six different 3D watermarking and steganographic methods are used for evaluating the performance of the proposed steganalytic methodology.

Keywords: 3D Objects, Steganalysis, Information Hiding, Watermarking, Steganography, Local Feature

1. Introduction

Computer graphics are becoming a more and more important medium in the interactive techniques such as Virtual Reality (VR) and 3D printing. In order to protect the copyright of the 3D objects, the digital watermarks maybe embedded into the 3D objects. 3D watermarking and steganographic algorithms seek to hide information in 3D objects, which can then be used for a variety of applications. Information is hidden in 3D objects for various purposes: copyright protection, defining behaviour characteristics similar to the DNA in beings, or hiding certain information for marketing purpose, etc. Moreover, the 3D objects can be the carriers of a covert communication channel when the 3D steganography is applied. While watermarking seeks to robustly embed rather smaller codes, steganography would embed larger payload messages without enforcing robustness. All these approaches aim to hide information in such a way that the changes they produce to the 3D objects are not visible. On the other hand steganalysis algorithms are being developed in order to find whether information is embedded in a certain media data. There are a lot of new steganalytic algorithms being proposed for audio signals [43, 31, 32], digital images [26, 12, 48, 36] and video [42, 37]. However, the steganalytic methods for 3D objects are far from sufficiently developed because of less attention but more challenges facing the task. While 3D objects can be represented in various ways, their most usual data representation is by means of meshes. Such irregular representations modelling complex 3D shapes are very different from the regular structural array representing audio, digital images or video. Consequently, the existing image and video steganalysis algorithms cannot be successfully applied to 3D objects.

Most research on 3D watermarking involves modifying certain geometrical properties of the object, most often in a statistical manner, in such a way that there are no visible changes. Research on 3D watermarking started in 1997 when Ohbuchi *et al.* proposed two 3D information hiding algorithms using ratios of local

*Corresponding author

Email addresses: zl991@york.ac.uk (Zhenyu Li), adrian.bors@york.ac.uk (Adrian G. Bors)

geometric measurements [30]. Cho *et al.* [10] proposed two blind robust watermarking algorithms based on modifying the mean or variance of the distribution of the vertices' radial distances in the spherical coordinate system. Cayre and Macq proposed a steganographic approach for 3D triangle meshes in [7] whose key idea is to consider each triangle from the mesh as a two-state geometrical object embedding a bit. A hierarchical 3D watermarking based on wavelet transform is proposed in [40]. This method embeds the robust, high-capacity and fragile watermark in different appropriate resolution levels obtained by wavelet decomposition of the mesh. Luo and Bors proposed changing the statistics of geodesic distance distributions in 3D objects [27]. The same authors proposed minimizing the surface distortions in 3D watermarking by using an optimization algorithm in [6]. Among the information hiding algorithms, we mention a multi-layer 3D steganographic method [8] which embeds large payloads using vertices' projections onto the principal axis of the object. This steganographic method can make use of several layers for embedding the information increasing thus significantly the embedded payload. However, not all bits embedded through this method are retrievable and some are lost. More recently, Yang *et al.* [47] proposed a steganalysis-resistant watermarking algorithm which embeds the payload by changing the histogram of the radial coordinates of the vertices. This watermarking method produces less embedding distortion in the 3D objects when compared to the methods proposed in [10]. A distortion-free steganographic algorithm [3] embeds the information into the meshes by permuting the order in which faces and vertices are stored. However, this algorithm is not robust to the vertex-reordering attack.

3D steganalysis only received very recently the attention of the scientific community. The 3D steganalysis approach proposed in [45] considered various features including the norms of vertices in the Cartesian and Laplacian coordinate systems [44], the dihedral angle of faces adjacent to the same edge, and the face normal. Parameters representing the statistics of these features were used as inputs to a quadratic classifier. Yang *et al.* [46], proposed a new steganalysis algorithm, specifically designed for the mean-based watermarking algorithm from [10]. This steganalysis algorithm first estimates the number of bins through exhaustive search and then detects the presence of the secret message by a tailor-made normality test. The ability of a steganalyzer to generalize from the training set to a large testing set is a very demanding requirement as well. A steganalytic approaches which is designed specially for addressing the cover source mismatch scenario in 3D steganalysis by selecting the features which are robust to the variations of the cover source was proposed in [25]. Cryptanalysis aspects of 3D watermarking in a larger context have been discussed in the review paper from [18].

The aims of a steganalyzer are difficult to achieve because the stego-object and cover-obejct are supposed to be almost identical under human visual observation assumptions. Different from the features and local descriptors [29] used for image and 3D object classification [39, 19], recognition [13] and retrieval [35, 49, 17, 50], which aim to recognise the content of the image or 3D object, the steganalytic features need to be invariant to the content of the image or 3D object but sensitive to the subtle artificial distortions in the local regions of the object. However, there are links between the steganalytic features and the measurements used for image and 3D object quality assessment[23, 41, 51]. For example, the local roughness measure proposed in [23] can detect the geometric noise on the surface, which resembles the embedding distortions caused by the information hiding methods. Additionally, the image gradient magnitude is both utilized for image quality assessment in [51] the colour image steganalysis [1].

In this paper, we propose some new features to be used for 3D steganalysis. For example, we use the Gaussian curvature and curvature ratio to capture the changes of the surface's curvatures. Furthermore, the vertex normal is also considered to find the alteration on the adjacent faces of each vertex. Finally, we propose the spherical coordinate features which include the coordinates of the vertex and the length of the edge in the spherical coordinate system. The spherical coordinate system is often utilized for hiding information in 3D objects, but it has not been exploited for 3D steganalysis yet. The statistics of sets of 3D features are then fed into machine learning algorithms, such as Fisher Linear Discriminant (FLD) ensemble [20], the most used classifier for image steganalysis. The discriminating ability for 3D steganalyzer trained with the proposed feature set is then compared against the one proposed in [45]. The description of the 3D steganalysis framework formulated in this study is provided in Section 2. The 3D feature set, used by the steganalyzer is presented in detail in Section 3. The experimental results are provided in Section 4, while the conclusions of this study are outlined in Section 5.

2. 3D Steganalysis Framework

In this section, we will give a brief introduction of the 3D steganalysis framework. The steganalysis framework is treated as a machine learning problem, consisting of training and testing stages. The training of the steganalyzer has the following processing steps: preprocessing, feature extraction and learning, as illustrated in Figure 1. These processing steps produce a parameter set discriminating between the 3D objects carrying hidden information and those that are not. The testing stage includes the same preprocessing and feature extraction steps as in the training stage, while applying the parameters learnt during the training on the features extracted from sets of test objects.

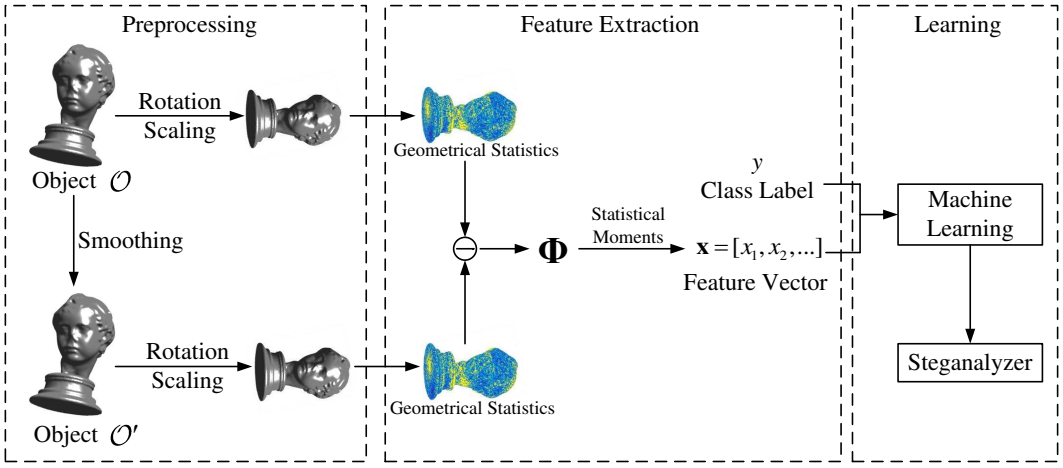

Figure 1: The 3D steganalysis framework based on learning from statistics of the local feature sets and classification by means of machine learning methods.

In the stage of preprocessing, a series of steps are applied to the object $\mathcal{O}$. Firstly, object $\mathcal{O}'$, a smoothed version of object $\mathcal{O}$, is obtained by using mesh smoothing, specifically Laplacian smoothing in this study. The idea of applying smoothing is based on the study in the image steganalysis. It was observed that the difference between the stego-image and its smoothed version is more significant than the difference between the cover-image and its corresponding smoothed version [15, 21]. Similarly, it is expected that the difference between a mesh and its smoothed version is larger for a stego mesh than for a cover mesh. In most 3D watermarking algorithms, the changes produced to the stego-object, following the watermark embedding can be associated to noise. Consequently, when smoothing a cover mesh, the resulting modifications will be smaller than those obtained when smoothing its corresponding stego mesh. We consider Laplacian smoothing, for both the object $\mathcal{O}$ and its smoothed version $\mathcal{O}'$. Then the rotation and scaling are used to normalize the objects such their size is constrained within a cube with sides of one, in order to eliminate the perturbation on the features cause by the variation of the sizes of the objects in the training set.

Features, characterizing the local geometry of 3D objects are extracted after the preprocessing process of the object $\mathcal{O}$. The discriminative features should be chosen such that they capture effectively the differences between the two versions of mesh for a given object. In Section 3 we propose to use a set of new 3D features for steganalysis. Then, $\mathbf{\Phi}$ is the difference between the geometrical statistics extracted from the cover-object $\mathcal{O}$ and the smoothed cover-object $\mathcal{O}'$, are compared with those of differences between the features extracted from the stego-object $\hat{\mathcal{O}}$ and its smoothed version $\hat{\mathcal{O}}'$, respectively. In order to model the differences, we consider the first four statistical moments, representing the mean, variance, skewness and kurtosis, of the logarithm of $\mathbf{\Phi}$ as the feature vector $\mathbf{x}$, which is used as inputs to machine learning algorithms along with y, the class label of object $\mathcal{O}$.

In the supervised learning phase, a classifier is learnt over the extracted feature vectors and the corresponding class labels of the objects. The classifier, which is also known as the steganalyzer, separates the

feature space defining the stego-objects from that of the cover-objects. Furthermore, choosing the appropriate machine learning algorithm and its training procedure are crucial, as steganalyzers trained by different machine learning methods can provide different results on identical training sets. In this research study we propose to use the FLD ensemble [20] for training the steganalyzer.

3. Features for 3D Steganalysis

3D watermarking and steganographic methods are specifically designed to embed information in a way that does not visibly alter the surface of the objects [27, 6]. Nevertheless, the changes produced in the 3D objects surface may be identified by steganalysis. Depending on the specific algorithm used, such changes could be randomly distributed on the surface of the 3D mesh [5] or they could be located specifically in certain regions of the object [2]. Artefacts produced in objects, following the information hiding procedure, could be assimilated to low level protuberances on mesh surfaces and consequently could be identified by feature detection algorithms. In the following we outline some 3D local features which can be used for identifying whether objects have been watermarked or not. Such feature detectors range from very simple vertex displacement measurements to algorithms that take into account the local neighbourhoods and measure specific shape characteristics.

Let us assume that we have a mesh representing the shape of a 3D object, considered as a cover mesh $\mathcal{O} = \{V, F, E\}$, containing the vertex sets $V = \{v(i)|i = 1, 2, \ldots, |V|\}$, where $|V|$ represents the number of vertices in the cover-object $\mathcal{O}$, its face sets F, and its edge sets E, respectively. We define the neighborhood of a vertex $v(i)$, the set of adjacent vertices $v^*(i) = \{v(j) \in V\}$

3.1. Preprocessing

As already mentioned in Section 2, the preprocessing of the 3D objects is an essential phase for extracting the steganalytic features. One iteration Laplacian smoothing is firstly applied to the 3D object $\mathcal{O}$. The vertex $v'(i)$ in smoothed object $\mathcal{O}'$ is formulated as follows [38]:

$$v'(i) \leftarrow v(i) + \frac{\lambda}{\sum_{v(j)\in v^*(i)} w_{ij}} \sum_{v(j)\in v^*(i)} w_{ij}(v(j) - v(i)), \tag{1}$$

where λ is a scale factor and w_{ij} are the weights defined as:

$$w_{ij} = \begin{cases} 1 & \text{if } v(j) \in v^*(i) \\ 0 & \text{otherwise} \end{cases} \tag{2}$$

.

An appropriate value of λ can be found through the experimental study so that the object can be smoothed in a proper extent. The smoothed 3D object is then rotated in order to align the x-axis and y-axis with the first and second principal axes of the vertices in the smoothed 3D object, respectively. Afterwards, the object is scaled to a unit cube, such that the largest span of the object in the three axes equals 1.

3.2. The YANG40 Features

The 40-dimensional feature vector YANG40 contains the most effective features from YANG208, used in [45], which correspond to the statistics of features evaluated from the vertices, edges and faces that make up the given meshes. For YANG40 we remove certain features, which provide lower performance, from YANG208 and abandon the strategy used in [45] which treats the vertices with valence less, equal, or greater than six separately to reduce the dimensionality.

Let us denote by $\mathbf{\Phi}$, the features representing differences between the cover-object $\mathcal{O}$ and its smoothed version $\mathcal{O}'$. The first six components of $\mathbf{\Phi}$ represent the absolute distance, measured along each coordinate

axis x, y, z between the locations of vertices of the meshes $\mathcal{O}$ and $\mathcal{O}'$, in both the Cartesian and Laplacian coordinate systems [44]:

$$\begin{aligned}\phi_1(i) &= |v_{x,c}(i) - {v'}_{x,c}(i)|,\\ \phi_2(i) &= |v_{y,c}(i) - {v'}_{y,c}(i)|,\\ \phi_3(i) &= |v_{z,c}(i) - {v'}_{z,c}(i)|,\end{aligned} \tag{3}$$

$$\begin{aligned}\phi_4(i) &= |v_{x,l}(i) - {v'}_{x,l}(i)|,\\ \phi_5(i) &= |v_{y,l}(i) - {v'}_{y,l}(i)|,\\ \phi_6(i) &= |v_{z,l}(i) - {v'}_{z,l}(i)|,\end{aligned} \tag{4}$$

where $v_{x,c}(i)$ and $v_{x,l}(i)$ represent the x-coordinate of $v(i)$ in Cartesian and Laplacian coordinate systems, respectively, $i = 1, 2, \ldots, |V|$. The Laplacian coordinates of the object are the result of the Cartesian coordinates multiplied by the *Kirchhoff* matrix [4] of the object. Next, we evaluate the changes produced in the Euclidean distance between vertex locations and the center of the object, representing the vertex norms. The absolute differences between the vertex norms of pairs of corresponding vertices in the meshes $\mathcal{O}$ and $\mathcal{O}'$ are calculated as:

$$\phi_7(i) = |\|\mathbf{v}_c(i)\| - \|\mathbf{v}'_c(i)\|| \tag{5}$$

$$\phi_8(i) = |\|\mathbf{v}_l(i)\| - \|\mathbf{v}'_l(i)\|| \tag{6}$$

where $\|\mathbf{v}_c(i)\|$, $\|\mathbf{v}_l(i)\|$, represent the vector norms in Cartesian and Laplacian coordinates, respectively, for $i = 1, 2, \ldots, |V|$.

Another feature evaluates the local mesh surface variation by calculating the changes in the orientations of faces adjacent to the same edge. This is measured by the absolute differences between the dihedral angles of neighbouring faces, calculated in the plane perpendicular on the common edge $\{e(i) \in \mathcal{O} | i = 1, 2, \ldots, |E|\}$, where $|E|$ represents the number of edges part of the object $\mathcal{O}$:

$$\phi_9(i) = |\theta_{e(i)} - \theta'_{e(i)}|, \tag{7}$$

where the calculation of the dihedral angle $\theta_{e(i)}$ is illustrated in Figure 2. Changes in the local surface orientation are measured by calculating the angle between the surface normals $\vec{N}_{F(i)}$, of the faces from the cover-object $F(i) \in \mathcal{O}$, and their correspondents $\vec{N}_{F'(i)}$, from the smoothed cover-object $F'(i) \in \mathcal{O}'$:

$$\phi_{10}(i) = \arccos \frac{\vec{N}_{F(i)} \cdot \vec{N}_{F'(i)}}{\left\|\vec{N}_{F(i)}\right\| \cdot \left\|\vec{N}_{F'(i)}\right\|} \tag{8}$$

where $i = 1, 2, \ldots, |F|$. The 40-dimensional feature vector YANG40 represents the first four statistical moments: mean, variance, skewness and kurtosis of the logarithm of the ten vectors $\{\phi_i | i = 1, 2, \ldots, 10\}$, described above.

3.3. The Vertex Normal and Curvature Features

In the following we propose to use some additional 3D features. The vertex normal is the weighted sum of the normals of all faces that contain the vertex [28]. A vertex normal is shown in Figure 2 and is computed as:

$$\vec{N}_{v(i)} = \sum_{F(j)} \frac{A(F(j)) \cdot \vec{N}_{F(j)}}{\|e_{(v(i),1)}\|^2 \cdot \|e_{(v(i),2)}\|^2} \tag{9}$$

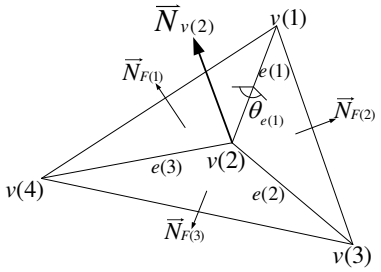

Figure 2: Dihedral angles and vertex-based normals for representing local geometry properties of the surface.

where $F(j)$ represents the j-th face that contains the vertex $v(i)$, $A(F(j))$ represents its area, $e_{(v(i),1)}$ and $e_{(v(i),2)}$ are the two edges containing $v(i)$ in the face $F(j)$. The change between the vertex normals is calculated as a dot product:

$$\phi_{11}(i) = \arccos \frac{\vec{N}_{v(i)} \cdot \vec{N}_{v'(i)}}{\left\|\vec{N}_{v(i)}\right\| \cdot \left\|\vec{N}_{v'(i)}\right\|} \tag{10}$$

where $\vec{N}_{v'(i)}$ is the normal for a vertex from the smoothed object $\{v'(i) \in \mathcal{O}' | i = 1, 2, \ldots, |V|\}$.

Next we consider the local shape curvatures, calculated according to the the Gaussian curvature and the curvature ratio formula used in [33]. In differential geometry, the two principal curvatures of a surface are provided by the eigenvalues of the shape operator, calculated at the location of a vertex using the vertices from its first neighbourhood. Such curvatures measure how the local surface bends by different amounts in orthogonal directions at that point. The Gaussian curvature is defined as:

$$K_G = K_1 K_2, \tag{11}$$

where K_1 is the minimum principal curvature and K_2 is the maximum principal curvature at a given point [34]. A special case is that of singularity in the shape operator, when we have a linear dependency in one direction or in both. In this case we have locally a planar region, which is characterized by a linear relationship among its coordinates and consequently by zero curvature. In our study we found that the curvature ratio proposed in [33], defined as

$$K_r = \frac{\min(|K_1|, |K_2|)}{\max(|K_1|, |K_2|)}, \tag{12}$$

is effective to be used as a feature when training steganalyzers. The Gaussian curvature from equation (11) and the curvature ratio from equation (12) have been shown to be sensitive to very small mesh modifications and have been used to model 3D shape characteristics in various applications. The two principal curvatures are evaluated at the location of each vertex in the cover-object $\mathbf{v}(i) \in \mathcal{O}$ and for its corresponding vertex from the smoothed object $\mathbf{v}'(i) \in \mathcal{O}'$. Their absolute differences represent the features ϕ_{12} and ϕ_{13}:

$$\phi_{12}(i) = |K_G(v(i)) - K_G(v'(i))|, \tag{13}$$

$$\phi_{13}(i) = |K_r(v(i)) - K_r(v'(i))|, \tag{14}$$

for $i = 1, 2, \ldots, |V|$.

3.4. The Spherical Coordinate Features

There are many information hiding algorithms would embed changes directly or indirectly in the spherical domain. Consequently, in the following we consider the spherical coordinate system for defining characteristics that can be used by the steganalyzers. We convert the 3D objects from the Cartesian coordinate system to the spherical coordinate system, considering the center of the object as its reference.

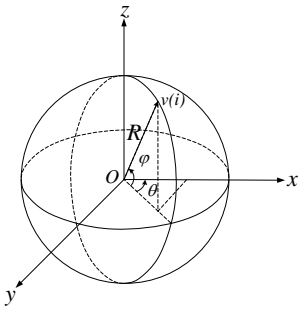

Figure 3: The spherical coordinate system, where R is the radial distance of vertex $v(i)$, θ and φ are its azimuth angle and elevation angle, respectively.

The spherical coordinate system specifies a point in the 3D space by a radius and two angles and the link to the Cartesian coordinate system is given by:

$$\begin{aligned} v_x &= R\cos(\varphi)\cos(\theta) \\ v_y &= R\cos(\varphi)\sin(\theta) \\ v_z &= R\sin(\varphi) \end{aligned} \tag{15}$$

where $\mathbf{v} = (v_x, v_y, v_z)$ represents the Cartesian coordinates of the vertex, and (R, θ, φ) its spherical coordinates, representing R, the Euclidean norm from a fixed origin, θ, the azimuth angle, while φ is the elevation angle, as illustrated in Figure 3. We compute the absolute differences of the spherical coordinates of all vertices, $\{(R(i), \theta(i), \varphi(i))$ between the original object $\mathcal{O}$ and the smoothed object $\mathcal{O}'$ in the spherical coordinate system:

$$\begin{aligned} \phi_{14}(i) &= |\theta(i) - \theta'(i)|, \\ \phi_{15}(i) &= |\varphi(i) - \varphi'(i)|, \\ \phi_{16}(i) &= |R(i) - R'(i)| \end{aligned} \tag{16}$$

where $i = 1, 2, \ldots, |V|$. The center of the spherical coordinate system is O, representing the center of the 3D object calculated by averaging all the vertices in the object, as shown in Figure 3.

We also use statistics of the edges, defined in the spherical coordinate system. In this case, edges are defined by the differences in the spherical coordinates of the two vertices that define the edge ends:

$$\begin{aligned} K_\theta(e_{(i,j)}) &= |\theta(i) - \theta(j)|, \\ K_\varphi(e_{(i,j)}) &= |\varphi(i) - \varphi(j)|, \\ K_R(e_{(i,j)}) &= |R(i) - R(j)| \end{aligned} \tag{17}$$

where $e_{(i,j)}$ is the edge connecting vertices $v(i)$ and $v(j)$, and $e_{(i,j)} \in E$. The corresponding features extracted from both the original object and its smoothed version are

$$\begin{aligned} \phi_{17}(i) &= |K_\theta(i) - K'_\theta(i)|, \\ \phi_{18}(i) &= |K_\varphi(i) - K'_\varphi(i)|, \\ \phi_{19}(i) &= |K_R(i) - K'_R(i)| \end{aligned} \tag{18}$$

where, for example, $K_\theta(i)$ is obtained from the i-th edge of the original object, while $K'_\theta(i)$ from its corresponding edge in the smoothed object, for $i = 1, 2, \ldots, |E|$, $|E|$ is the total number of edges in object $\mathcal{O}$.

Firstly, we apply the logarithm on all features in order to reduce the range of their values and enforce a degree of evenness in their distribution. After applying the logarithm, we consider the four statistical

moments, representing the mean, variance, skewness and kurtosis, of the logarithm of all the vertex normals, Gaussian curvatures, curvature ratios, and the spherical coordinate features calculated as indicated above, as in the case of the feature set YANG40, defined in Section 3.2. In this way we define a vector $\mathbf{x}$ of $19 \times 4 = 76$ dimensions, which we call LFS76. The four order moments capture almost entirely the statistical characteristics of the distribution of the features, representing their center and the deviation from the center, as indicated by the mean and variance, respectively. The degree of symmetry in the logarithm of feature values is indicated by the skewness, while the level of peakedness and the presence of specific values in the statistical distribution is indicated by the kurtosis.

A subset of the proposed features set, LFS52, was used in [24]. That feature set did not include the 24-dimensional feature vector extracted in the spherical coordinate system of 3D objects. A higher dimensional feature set, used in [45], is represented by the 208-dimensional vector defined as YANG208. This feature set considers separately the statistics of the first eight features described above, distinctly on vertex sets with valences less, equal, or greater than six. Moreover, YANG208 feature set considers the histogram differences of the ten features defined in Section 3.2, as well.

4. Experimental results

In the following we provide the experimental results of the proposed 3D steganalytic methodology, when detecting the stego-objects obtained by six different information hiding methods. For the experiments we use the Princeton Mesh Segmentation project [9] database, which consists of 354 3D objects represented as meshes. The shapes of ten objects from this database are shown in Figure 4.

Figure 4: 3D objects used in the steganalytic tests.

4.1. The 3D information hiding methods and parameter settings

During the tests we consider detecting the 3D stego-objects obtained by six different information hiding methods: the Steganalysis-Resistant Watermarking (SRW) method proposed in [47]; the two blind robust watermarking algorithms based on modifying the Mean or the Variance of the distribution of the vertices' Radial distances in the Spherical coordinate system, denoted as MRS and VRS, from [10]; the Wavelet-based High Capacity (WHC) watermarking method and Wavelet-based FRagile (WFR) watermarking method proposed in [40]; the Multi-Layer Steganography (MLS) provided in [8].

During the generation of the stego-objects using SRW method from [47], we consider multiple values for the parameter K which determines the number of bins in the histogram of the radial distance of the vertex. According to [47], the upper bound of the embedding capacity is $\lfloor (K-2)/2 \rfloor$. In our experiments we set the parameter $K = \{32, 64, 96, 128\}$ and thus obtain multiple sets of stego-objects. Another parameter in the watermarking method from [47] is n_{thr} which controls the robustness of the embedding method. In order to keep the distortion of the embedding to a relatively low level, we set the parameter n_{thr} as 20. If the smallest number of the elements in the bins from the objects is less than 20, we would choose n_{thr} equal to

the smallest nonzero number of the elements in the bins. Examples of stego-objects obtained using SRW method are shown in Figure 7 (a) and Figure 8 (a), where $K = 128$.

For MRS and VRS watermarking methods from [10], we consider various values for the watermark strength, such as $\alpha = \{0.02, 0.04, 0.06, 0.08, 0.1\}$, while fixing the incremental step size to $\Delta k = 0.001$ and the message payload as 64 bits. Larger value of the strength can increase the robustness of the watermark, but also enlarge the extent of the embedding modifications. An example of a stego-object obtained using MRS method is shown in Figure 7 (f), where the watermark strength factor is set as $\alpha = 0.04$.

In terms of WHC and WFR watermarking methods from [40], the information are both embedded in the wavelet coefficient vectors obtained just after one wavelet decomposition of the original mesh, but the modifications are made by different ways. During the watermark embedding by WHC, the wavelet coefficient vectors' norms are divided by the parameter p firstly. Then the obtained residues are changed accordingly to generate a particular permutation which carries the watermark. The parameter p is obtained by dividing the averaged edge length by the control parameter ϵ_{hc}, which is set to {50, 100, 500, 1000} in the experiment. When using WFR to embed information, the angle between the wavelet coefficient vector and its associated edge is changed, where Δ_θ is the quantization step used to establish the codebook. To investigate the influence of parameter Δ_θ on the steganalysis results, we set it to $\{\pi/6, \pi/4, \pi/3, \pi/2\}$. The other parameters involved in WHC and WFR are all exactly set to the values suggested in the experimental part of the literature [40].

When using MLS method from [8], we increase the number of layers from 2 to 10, with the step of 2, and we consider the number of intervals as 10000. Increasing the number of embedding layers in this steganographic method corresponds to increasing the payload capacity. During the embedding, all the vertices in the mesh are used as payload carriers, except for three vertices which are used as references for the extraction process. A stego-object obtained using the MLS method is shown in Figure 7 (k), where the number of layers is 10.

4.2. Feature extraction

The steganalytic features are extracted from the cover-objects and the corresponding stego-objects embedded with information by the six embedding algorithms introduced above. During the preprocessing, we first apply one iteration of Laplacian smoothing on both cover-objects and stego-objects, by setting the scale factor $\lambda = 0.2$, which appears to provide good performance for most of the cases. We consider the proposed feature set LFS76, discussed in Section 3 and compare their results against YANG208, proposed in [45], its simplified version, called YANG40, and LFS52 proposed in our previous work [24]. We also consider the feature sets combining LFS52 and the features about the Vertices' Spherical coordinates, VS12, representing the mean, variance, skewness and kurtosis of ϕ_{14}, ϕ_{15} and ϕ_{16} from equation (16), the combination of LFS52 and features about the Edge length in the Spherical coordinate system, ES12, representing the mean, variance, skewness and kurtosis of ϕ_{17}, ϕ_{18} and ϕ_{19} from equation (18).

Figures 5 (a) and (b) show the histograms of the dihedral angles feature ϕ_9, calculated according to equation (7), for the cover-object and stego-object, respectively, for the object "Head statue" shown in Figure 7 (f). The histograms of the logarithm of ϕ_9 are shown in Figures 5 (c) and (d), for the cover-object and stego-object, respectively. Figures 6 (a) and (b) show the histograms of the vertex normal feature ϕ_{11} calculated according to equation (10), while Figures 6 (c) and (d) show the corresponding histogram of logarithms for the cover-object "Horse" shown in Figure 4, and its corresponding stego-object embedded by MRS method from [10]. From these figures, we can observe following the application of the logarithm, the distributions of feature components ϕ_9 and ϕ_{11} become similar to that of normal distributions where it is easier to model the differences between the geometrical statistics of the cover-object and stego-object when using the four statistical moments of mean, variance, skewness and kurtosis.

Figures 7 (a) (f) and (k) are the stego-objects embedded by the information hiding methods, SRW [47], MRS [10] and MLS [8], respectively. Figure 8 (a) is the stego-object obtained by using SRW method. From the second to the fifth column of Figures 7 and 8 illustrate the absolute differences of the features between the cover-object and its corresponding stego-object, namely, vertex normals ϕ_{11}, the curvature ratios ϕ_{13}, the azimuth angles ϕ_{14} and the radial distances ϕ_{16}, depicted on the stego-objects. From these figures it

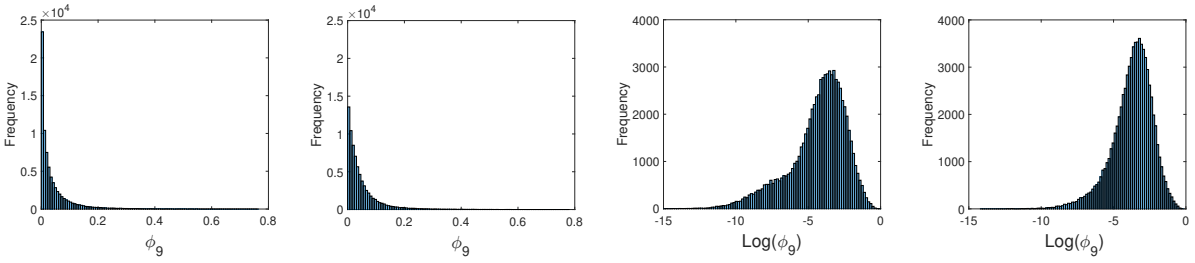

(a) Cover (b) Stego (c) Cover (d) Stego

Figure 5: Histograms of dihedral angles feature ϕ_9 and its logarithm of the cover and stego versions of the "Head statue" object from the database from [9].

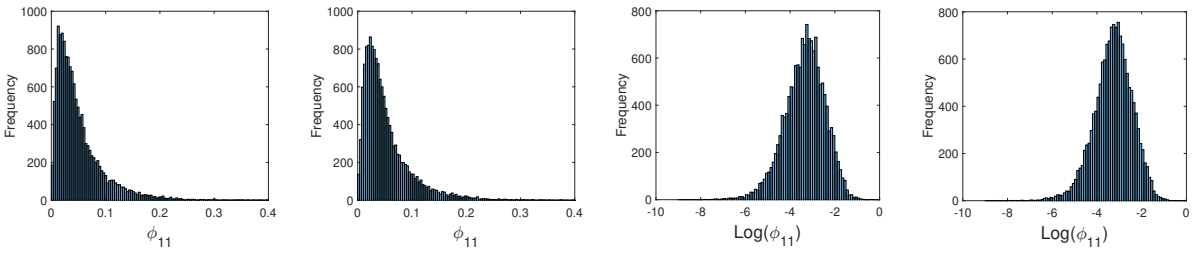

(a) Cover (b) Stego (c) Cover (d) Stego

Figure 6: Histograms of vertex normal feature ϕ_{11} and its logarithm of the cover and stego versions of the "Horse" object from the database from [9].

can be observed that each feature identifies specific differences between the cover-object and stego-object, which usually does not overlap with others.

4.3. Training steganalyzers

The steganalyzers are trained as binary classifiers implemented using two methods: the Quadratic Discriminant Analysis (QDA), Fisher Linear Discriminant (FLD) ensemble. The quadratic discriminant that fits multivariate normal densities with covariance estimates [22] was used in [45] as well. The FLD ensemble classifier was successfully used in image steganalysis [20, 12, 48]. The FLD ensemble consists of a set of base learners trained uniformly on the randomly selected feature subset of the whole training data. The dimensionality of the random subspace and the number of base learners is found by minimizing the out-of-bag (OOB) error, representing an estimate of the testing error calculated on bootstrap samples of the training set, [14]. Compared to the SVM classifier, the FLD ensemble can provide a comparable high accuracy, but with a relatively low computational cost, and it is much easier to find the optimal parameters for FLD ensemble. For more technical details of the FLD ensemble, we refer to the literature [20, 11]

For each steganalyzer, we split the 354 pairs of cover-object and stego-object into 260 pairs, used for training, and 94 pairs for testing. We consider 30 different splits of the given 3D object database, into the training and testing data sets. The results are given by considering two measurements. The first one is the median value of the detection errors, which is the average of false negatives (missed detections) and false positives (false alarms) from all 30 trials, while the other one is the median value of the area under the Receiver Operating Curves (ROC) of the detection results, evaluated over the 30 splits of the data into training and testing sets.

4.4. Steganalysis of the information hiding methods

For each information hiding method mentioned earlier in this section, two types of steganalyzers, FLD ensemble classifier and QDA classifier, are trained over the proposed feature sets. Figure 9 shows the

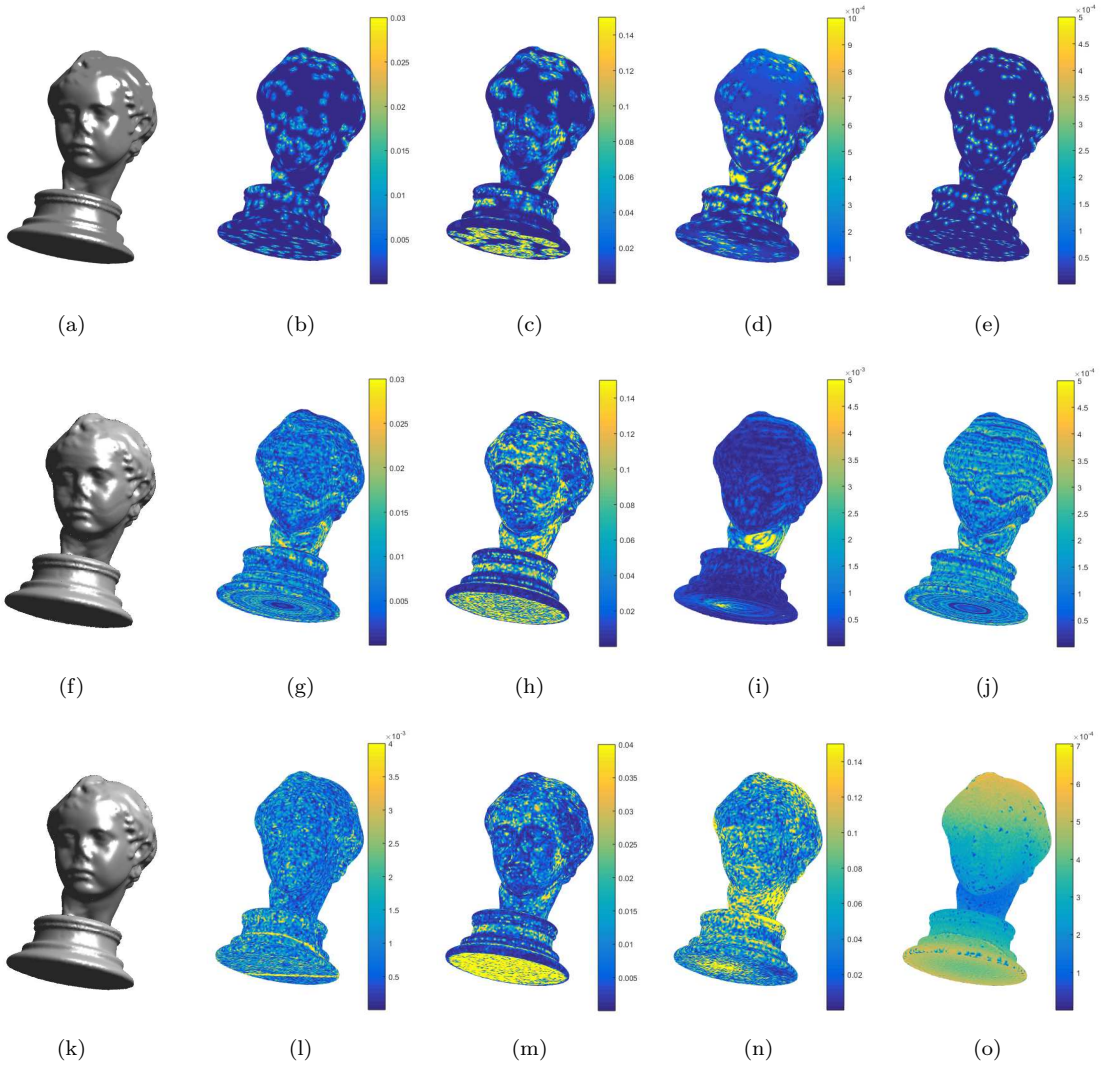

Figure 7: Stego-objects and the visualization of differences in the detection of features used for steganalysis. (a), (f) and (k) are the stego-objects obtained after using the information hiding algorithms, SRW [47], MRS [10] and MLS [8], respectively; (b), (g) and (l) show the absolute differences of vertex normals ϕ_{11} between those stego-objects and their corresponding cover-object, respectively; (c), (h) and (m) for the curvature ratios ϕ_{13}; (d), (i) and (n) for the azimuth angle ϕ_{14}; (e), (j) and (o) for the radial distance ϕ_{16}.

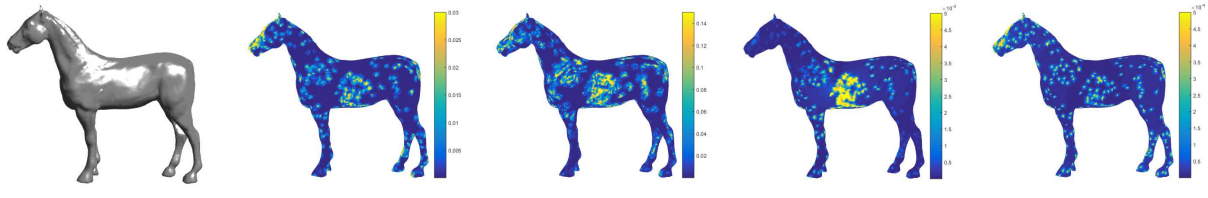

Figure 8: Stego-object and the visualization of differences in the detection of features used for steganalysis. (a) The stego-object obtained after using SRW algorithms described in [47]; (b) The absolute differences of vertex normals ϕ_{11} between the stego-objects and their corresponding cover-object; The absolute differences in (c) for the curvature ratios ϕ_{13}; (d) for the azimuth angle ϕ_{14}; (e) for the radial distance ϕ_{16}.

detection errors for the six information hiding methods, SRW [47], MRS [10], VRS [10], WHC [40], WFR [40] and MLS [8], using the FLD ensemble classifier, trained with the six combinations of feature sets, formed as mentioned above. It can be seen from Figure 9 that the LFS76 shows best performance among the six combinations for most of the cases. The improvement of the efficiency of LFS76, compared to YANG208, is quite evident for all the six embedding algorithms. The advantage of LFS76 over LFS52 is more obvious when detecting SRW, MRS and VRS methods, than detecting WHC, WFR and MLS methods. This is because WHC, WFR and MLS methods from do not produce the modifications in the spherical coordinate system, which makes the spherical coordinate features, VS12 and ES12, less useful for detecting the changes produced by embedding in these cases. Comparing the VS12 and ES12, it appears that usually the combination of LFS52 and ES12 achieves better performance than that of LFS52 and VS12, which means ES12 is more efficient than VS12.

In Figure 9 (a), we have observed that as the value of K increases, the detection error for SRW [47] tends to increase as well. This happens because the larger K will lead to fewer elements in each bin, so less vertices need to be changed for embedding a single bit. From Figures 9 (b) and (c) we can observe that as the watermarking strength of MRS and VRS [10] increases, all steganalyzers provide better detection accuracy. This is due to the fact that more significant changes are produced in the 3D object surface, which is caused by watermarks that have stronger embedding parameters. For WHC [40] method, the detection error shown in Figure 9 (d) increases slightly when ϵ_{hc} ranges from 50 to 100, but remains stable afterwards. In Figure 9 (e), the detection error for WFR [40] method does not have obvious changes when the parameter Δ_θ varis, which indicates the parameter Δ_θ does not influence the embedding distortion of the object seriously. It can be observed from Figure 9 (f) that the detection error for MLS [8] does not decline when the embedding capacity increases. The reason for this is that, according to the multi-layer embedding framework applied in [8], the distortions produced to the objects are always controlled in a fixed extent during the embedding.

Figure 10 shows the detection errors for the six information hiding methods, using the QDA classifier, trained with the multiple combinations of feature sets. The trends of the detection errors for the six embedding algorithms depicted in Figure 10 are similar to those shown in Figure 9, but the performance of the QDA classifier is not as good as the FLD ensemble classifier in general.

In the following, we discuss the undetectability of the six information hiding algorithms with respect to the steganalyzers trained with LFS76 feature set. When $K = 128$, the payload of SRW is close to 64 bits, which is the payload of MRS and VRS in our experiment. From Figures 9 (a) (b) and (c) we can see that SRW has an higher undetectability than those of MRS and VRS which is also reported in [47]. Since the procedure and embedding domain of MRS and VRS are very similar, it is not surprising that their undetectabilitis are close to each other. WHC and WFR also have quite similar undetectabilitis, which are higher than those of the other four information hiding algorithms in the experiment. We infer that is because LFS76 dose not include the features from the wavelet domain, the domain modifications are made by WHC and WFR, of the 3D object. The undetectability of MLS is moderate among the six information hiding methods according to the Figure 9, but the payload of MLS can be much higher than the other methods, approximate to 10 times of the number of the vertex in the object. If the payload of MLS reduce to 64 bits per object, the stego-objects embedded by MLS will be much harder to be detected.

4.5. Analysing the efficiency of features for steganalysis

In order to investigate the contribution of different categories of features from the set LFS76 to the steganalysis, we use the relevance between the feature vectors and the class label in order to assess each feature's efficiency. The measurement of the relevance is addressed by using the Pearson correlation coefficient,

$$\rho(x_i, y) = \frac{cov(x_i, y)}{\sigma_{x_i}\sigma_y} \tag{19}$$

where x_i is the i-th feature of a given feature set, $\mathbf{x} = \{x_i | i = 1, 2, \ldots, N\}$, and N is the dimensionality of the input feature, y is the class label indicating whether the class corresponds to a cover-object or a stego-object, cov represents the covariance and σ_{x_i} is the standard deviation of x_i. The Pearson correlation coefficient is well known as a measure of the linear dependence between two variables [16]. Then we set

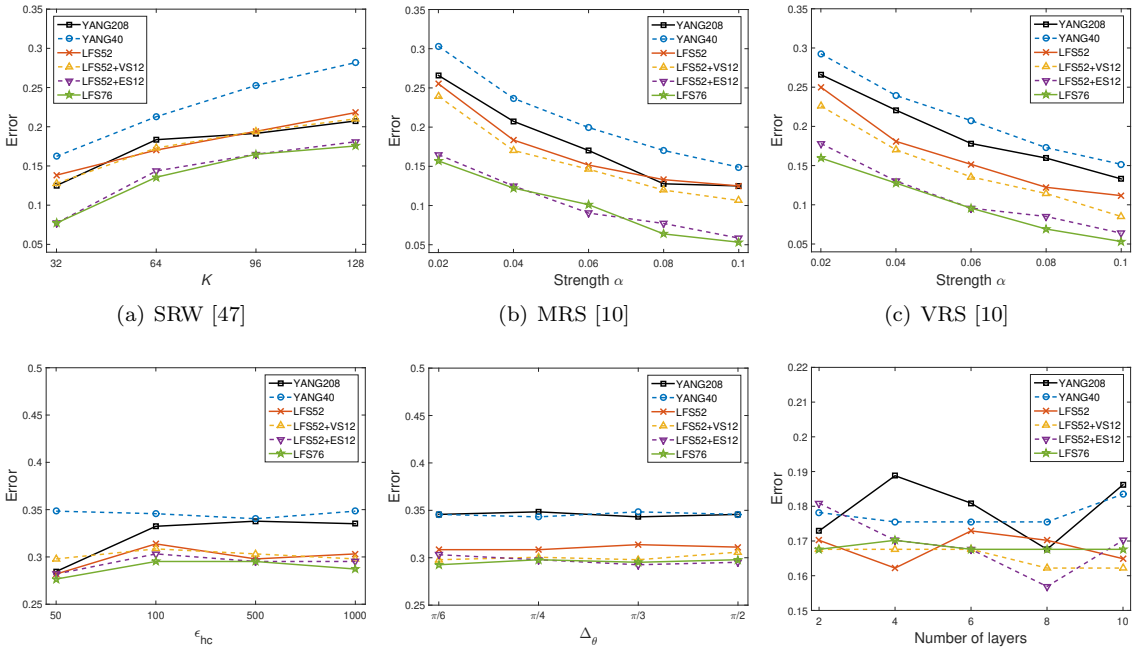

(a) SRW [47] (b) MRS [10] (c) VRS [10]

(d) WHC [40] (e) WFR [40] (f) MLS [8]

Figure 9: Median value of detection errors of the steganalyzers trained as FLD ensembles classifier on the testing set over 30 independent splits for the six information hiding methods with different values for parameters.

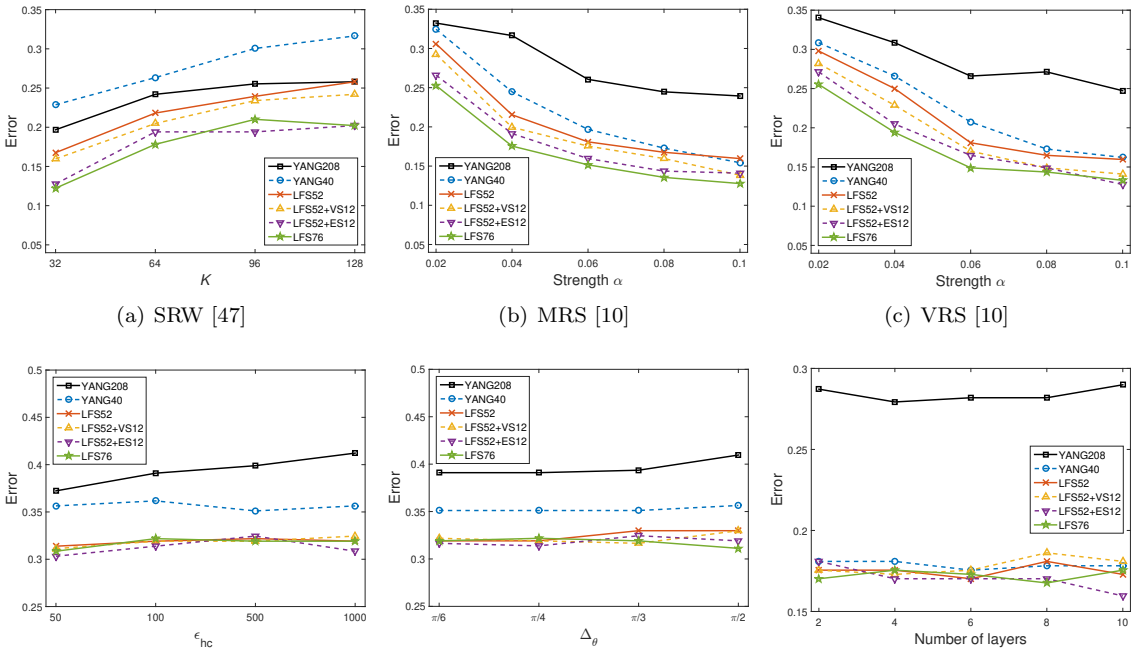

(a) SRW [47] (b) MRS [10] (c) VRS [10]

(d) WHC [40] (e) WFR [40] (f) MLS [8]

Figure 10: Median value of detection errors of the steganalyzers trained as QDA classifier on the testing set over 30 independent splits for the six information hiding methods with different values for parameters.

$|\rho(x_i, y)|$ as the value of the relevance, where $|\rho(x_i, y)| = 1$ indicates a highly linear relationship between the feature and the class label, corresponding to a better discriminant ability of that feature.

The analysis is conducted on the features extracted from the 354 cover-objects used above and six sets of corresponding stego-objects which are produced by the six watermarking and steganographic algorithms, SRW, MRS, VRS, WHC, WFR and MLS, respectively. We set the parameter K in SRW algorithm from [47] as 128. For the two watermarking methods, MRS and VRS, from [10], in order to find a balance between the watermarking strength and its undetectability, we set the watermarking strength as 0.04 and embed a payload of 64 bits. For WHC and WFR methods, we set the parameters as $\epsilon_{hc} = 100$ and $\Delta_\theta = \pi/6$, which are the same as the settings in [40]. In the case when using MLS method from [8], we consider ten layers of embedding.

We split the features from the set LFS76 into 10 categories according to their representation of the local shape geometry: 1, the vertex coordinates in the Cartesian coordinate system (ϕ_1, ϕ_2 and ϕ_3); 2, the vertex norm in the Cartesian coordinate system (ϕ_7); 3, the vertex coordinates in the Laplacian coordinate system (ϕ_4, ϕ_5 and ϕ_6); 4, the vertex norm in Laplacian coordinate system (ϕ_8); 5, the face normal (ϕ_{10}); 6, the dihedral angle (ϕ_9); 7, the vertex normal (ϕ_{11}); 8, the curvature (ϕ_{12} and ϕ_{13}); 9, the vertex coordinates in spherical coordinates system (ϕ_{14}, ϕ_{15} and ϕ_{16}); 10, the edge length in the spherical coordinate system (ϕ_{17}, ϕ_{18} and ϕ_{19}).

The relevance for all features from LFS76, is calculated according to equation (19), and the averaged relevances of the features in each category are shown in Figure 11. From Figure 11 we can observe that the new proposed features, represented by labels 7, 8 and 10, have relatively high relevance to the class label. More specifically, in Figure 11 (a), the features characterizing the local curvature (label 8) achieve the highest relevance. The relevance of the proposed ES12 feature, represented by labels 10, is higher than that of the proposed VS12 represented by labels 9. This implies that the efficiency of ES12 is higher than ES12, which is also reflected in the Figures 9 and 10. Comparing the formulation of VS12 and ES12, it is noted that two adjacent vertices are taken into account when extracting the ES12 features. However, the vertices in the object are considered individually in the case of VS12. So ES12 maybe more capable of capturing the distortion in the local region caused by the embedding modifications than VS12. However, the VS12 probably provides complementary information to the ES12, resulting in better performance of LFS76 than the combination of LFS52 and ES12 shown in the Figures 9 and 10. Meanwhile, in Figures 11, the vertex normal feature (label 7) and the face normal feature (label 5) obtain similar level of relevance, which is because the vertex normal is dependent on face normal in equation (9).

It is interesting that the relevance of the dihedral angle feature (label 6) shows high relevance to the class label in the cases of MRS, VRS and MLS, but shows much lower relevance when the stego-objects are generated by SRW, WHC and WFR methods. This may happen because almost all vertices from a mesh are slightly changed by MRS, VRS and MLS methods, while such changes are scattered among the vertices in the case of SRW method from [47], as it can be observed from Figures 7 (b) (g) and (l). Similarly in the cases of WHC and WFR, since the modification are made after only one wavelet decomposition, so just half of the vertices on the objects are possible to be modified, which preserves the dihedral angles to some extent. It is noticed that the features representing the vertex coordinates and norm in the Laplacian coordinate system (labels 3 and 4) have much higher relevance than those representing the vertex coordinates and norm in the Cartesian coordinate system (labels 1 and 2). According to the description of the Laplacian coordinate system in [44], the Laplacian coordinates of a vertex are based on the position of the vertex and adjacent vertices, which capture the geometrical information of a larger region than the Cartesian coordinates for each vertex.

In the following, we increase the feature set used for training steganalyzer gradually, from YANG40 to LFS52, adding either VS12 or ES12 to LFS52, and finally LFS76, and compare with YANG208. YANG40 includes the features represented by labels 1-6 in Figure 11. Features represented by labels 1-8 form LFS52 , while labels 1-10 correspond to LFS76. VS12 and ES12 are represented by labels 9 and 10, respectively. We used FLD ensemble and QDA as the learning method to train the steganalyzers for the six information hiding methods mentioned above. The performance of the feature sets are evaluated by the area under the ROC curves of the corresponding steganalyzers. A larger area under the ROC curve means that the classifier has a better detection accuracy.

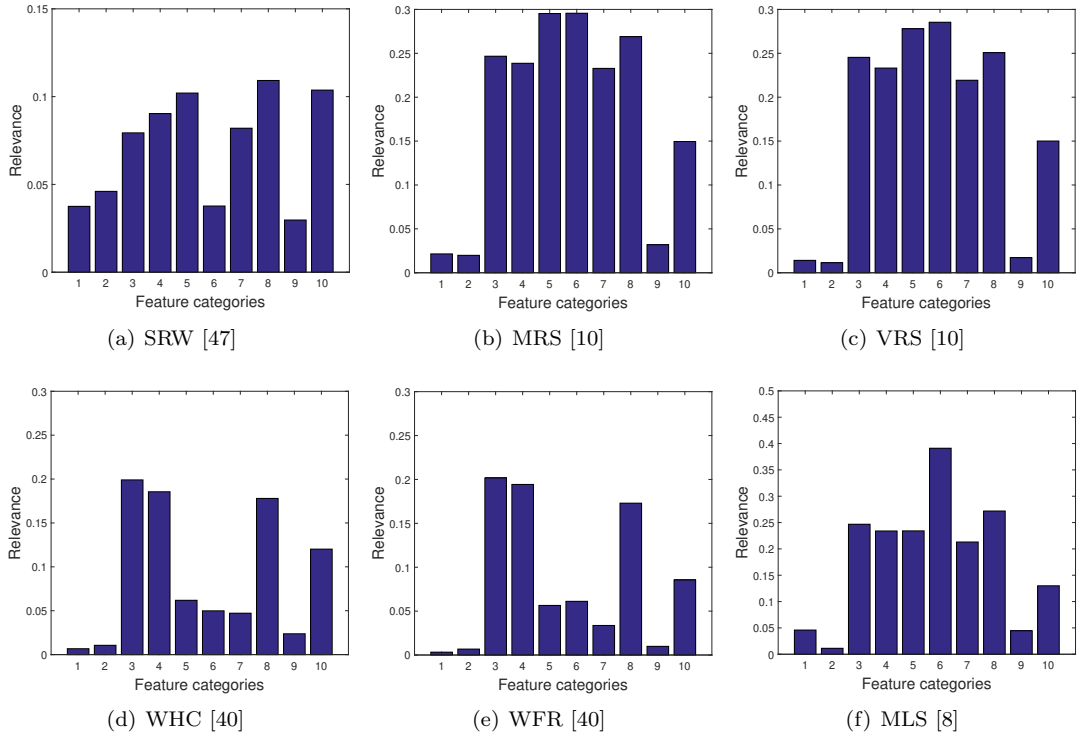

(a) SRW [47] (b) MRS [10] (c) VRS [10]

(d) WHC [40] (e) WFR [40] (f) MLS [8]

Figure 11: The relevance between the features and the class label, cover (0) or stego (1), where the stego objects are generated by the six information hiding methods, SRW, MRS, VRS, WHC, WFR and MLS, respectively. The meaning of the category labels are: 1, the vertex coordinates in Cartesian coordinate system; 2, the vertex norm in Cartesian coordinate system; 3, the vertex coordinates in Laplacian coordinate system; 4, the vertex norm in Laplacian coordinate system; 5, the face normal; 6, the dihedral angle; 7, the vertex normal; 8; the curvature; 9, the vertex coordinates in spherical coordinates system; 10, the edge length in spherical coordinate system.

Table 1: Median values of the area under the ROC curves for the steganalysis results of the six information hiding algorithms when using the FLD ensemble classifier.

Feature sets	Information hiding methods					
	SRW[47]	MRS[10]	VRS[10]	WHC[40]	WFR[40]	MLS[8]
YANG208	0.8781	0.8745	0.8748	0.7403	0.7320	0.9138
YANG40	0.7782	0.8167	0.8076	0.7048	0.7233	0.9207
LFS52	0.8621	0.8857	0.8902	0.7633	0.7732	0.9254
LFS52+VS12	0.8617	0.8999	0.9037	0.7676	0.7845	**0.9297**
LFS52+ES12	**0.9064**	0.9496	0.9414	0.7770	0.7905	0.9184
LFS76	0.9032	**0.9544**	**0.9466**	**0.7858**	**0.7963**	0.9269

Table 2: Median values of the area under the ROC curves for the steganalysis results of the six information hiding algorithms when using the QDA classifier.

Feature sets	Information hiding methods					
	SRW[47]	MRS[10]	VRS[10]	WHC[40]	WFR[40]	MLS[8]
YANG208	0.8035	0.7871	0.7888	0.6651	0.6730	0.8482
YANG40	0.7485	0.8573	0.8395	0.7118	0.7285	0.8834
LFS52	0.8228	0.8770	0.8518	0.7600	0.7394	0.8697
LFS52+VS12	0.8351	0.8886	0.8721	0.7467	0.7530	0.8697
LFS52+ES12	0.8702	0.8797	0.8829	0.7551	**0.7594**	**0.8909**
LFS76	**0.8871**	**0.8907**	**0.8895**	**0.7610**	0.7590	0.8692

Tables 1 and 2 provide the median values of the area under the ROC curves for the steganalytic methods when using six combinations of feature sets for 30 independent splits of the training/testing set. It can be seen from Table 1 that the areas under the ROC curves of the steganalyzers increase with the addition of new features, such as vertex normal features and curvature features, to the YANG40 feature set. After adding VS12 and ES12 to LFS52 feature set, the LFS76 feature set achieves the best performance for most of the cases. For SRW and MLS, the combination of LFS52 and ES12 and that of LFS52 and VS12 obtain the best performance, respectively, which also justifies the importance of VS12 and ES12 features. But in general, the combination of LFS52 and ES12 has a better performance than that of LFS52 and VS12, indicating the higher efficiency of ES12 than VS12, consistently reflected in Figure 11. The upward trend in the area under the ROC curves along with addition of new features also exists in Table 2. However, it is obvious that the QDA classifier, used in [45], does not achieve the so good performance as the FLD ensemble classifier in general.

5. Conclusion

The task of a 3D steganalyzer is very challenging because it has to find very small differences between stego-obejcts and cover-objects. In this research study, we propose to use the statistics of some new shape features as inputs for 3D steganalyzers. We analyze various local features used for 3D steganalysis by evaluating their relevance to the class label and by testing their performance in the experiments. The first four statistical moments in various 3D feature sets are used for training steganalyzers by two machine learning methods, namely, the quadratic discriminant and Fisher Linear Discriminant (FLD) ensemble. After training, these steganalyzers are used for differentiating the stego-objects from the cover-objects. The experimental results show that the proposed 3D feature sets provide the best results for the steganalysis of six 3D information hiding algorithms. Since the detection errors for the wavelet-based embedding algorithms, such as WHC and WFR, are higher than those for the other embedding algorithms, in future studies we will try to improve the detection performance for WHC and WFR by extracting the features from the wavelet domain of 3D object. In addition, we will assess the generalization ability of the proposed 3D steganalyzers.

Acknowledgements

The authors would like to thank the anonymous editor and reviewers for their constructive comments. The first author acknowledges the scholarship received from Zhengzhou Institute of Information Science and Technology.

References

[1] Abdulrahman, H., Chaumont, M., Montesinos, P., Magnier, B.. Color image steganalysis based on steerable gaussian filters bank. In: Proceedings of the 4th ACM Workshop on Information Hiding and Multimedia Security. ACM; 2016. p. 109–114.

[2] Alface, P.R., Macq, B., Cayre, F.. Blind and robust watermarking of 3-D models: How to withstand the cropping attack? In: Proc. of IEEE Int. Conf. Image Processing. 2007. p. 465–468.

[3] Bogomjakov, A., Gotsman, C., Isenburg, M.. Distortion-free steganography for polygonal meshes. Computer Graphics Forum 2008;27(2):637–642.

[4] Bollobás, B.. Modern graph theory. volume 184. Springer Science & Business Media, 2013.

[5] Bors, A.G.. Watermarking mesh-based representations of 3-D objects using local moments. IEEE Transactions on Image Processing 2006;15(3):687–701.

[6] Bors, A.G., Luo, M.. Optimized 3D watermarking for minimal surface distortion. IEEE Transactions on Image Processing 2013;22(5):1822–1835.

[7] Cayre, F., Macq, B.. Data hiding on 3-D triangle meshes. IEEE Transactions on Signal Processing 2003;51(4):939–949.

[8] Chao, M.W., Lin, C.h., Yu, C.W., Lee, T.Y.. A high capacity 3D steganography algorithm. IEEE Transactions on Visualization and Computer Graphics 2009;15(2):274–284.

[9] Chen, X., Golovinskiy, A., Funkhouser, T.. A benchmark for 3D mesh segmentation. ACM Transactions on Graphics 2009;28(3):73:1–73:12.

[10] Cho, J.W., Prost, R., Jung, H.Y.. An oblivious watermarking for 3-D polygonal meshes using distribution of vertex norms. IEEE Transactions on Signal Processing 2007;55(1):142–155.

[11] Cogranne, R., Fridrich, J.. Modeling and extending the ensemble classifier for steganalysis of digital images using hypothesis testing theory. IEEE Transactions on Information Forensics and Security 2015;10(12):2627–2642.
[12] Denemark, T.D., Boroumand, M., Fridrich, J.. Steganalysis features for content-adaptive JPEG steganography. IEEE Transactions on Information Forensics and Security 2016;11(8):1736–1746.
[13] Ding, C., Xu, C., Tao, D.. Multi-task pose-invariant face recognition. IEEE Transactions on Image Processing 2015;24(3):980–993.
[14] Duda, R.O., Hart, P.E., Stork, D.G.. Pattern classification. John Wiley & Sons, 2012.
[15] Fridrich, J.J., Goljan, M., Hoga, D.. Steganalysis of JPEG images: Breaking the f5 algorithm. In: Proc. of Workshop of Information Hiding, LNCS, vol. 2578. 2002. p. 310–323.
[16] Hall, M.A.. Correlation-based Feature Selection for Machine Learning. Ph.D. thesis; The University of Waikato; 1999.
[17] Hong, C., Yu, J., Tao, D., Wang, M.. Image-based three-dimensional human pose recovery by multiview locality-sensitive sparse retrieval. IEEE Transactions on Industrial Electronics 2015;62(6):3742–3751.
[18] Itier, V., Puech, W., Bors, A.G.. Cryptanalysis aspects in 3-D watermarking. In: Proc. of IEEE Int. Conf. on Image Processing. 2014. p. 4772–4776.
[19] Kannala, J., Rahtu, E.. Bsif: Binarized statistical image features. In: Pattern Recognition (ICPR), 2012 21st International Conference on. IEEE; 2012. p. 1363–1366.
[20] Kodovskỳ, J., Fridrich, J., Holub, V.. Ensemble classifiers for steganalysis of digital media. IEEE Transactions on Information Forensics and Security 2012;7(2):432–444.
[21] Kodovsky, J., Fridrich, J.J.. Calibration revisited. In: Proc. of ACM workshop on Multimedia and Security. 2009. p. 63–74.
[22] Krzanowski, W.. Principles of multivariate analysis. Oxford University Press, 2000.
[23] Lavoué, G.. A local roughness measure for 3d meshes and its application to visual masking. ACM Transactions on Applied perception (TAP) 2009;5(4):21.
[24] Li, Z., Bors, A.G.. 3D mesh steganalysis using local shape features. In: Proc. of IEEE Int. Conf. on Acoustics, Speech and Signal Processing (ICASSP). 2016. p. 2144–2148.
[25] Li, Z., Bors, A.G.. Selection of robust features for the cover source mismatch problem in 3D steganalysis. In: Proc. of the 23rd Int. Conf. on Pattern Recognition. IEEE; 2016. p. 4251–4256.
[26] Li, Z., Hu, Z., Luo, X., Lu, B.. Embedding change rate estimation based on ensemble learning. In: Proc. of ACM workshop on Information Hiding and Multimedia Security. ACM; 2013. p. 77–84.
[27] Luo, M., Bors, A.G.. Surface-preserving robust watermarking of 3-D shapes. IEEE Transactions on Image Processing 2011;20(10):2813–2826.
[28] Max, N.. Weights for computing vertex normals from facet normals. Journal of Graphics Tools 1999;4(2):1–6.
[29] Mikolajczyk, K., Schmid, C.. A performance evaluation of local descriptors. IEEE transactions on pattern analysis and machine intelligence 2005;27(10):1615–1630.
[30] Ohbuchi, R., Masuda, H., Aono, M.. Embedding data in 3D models. In: Interactive Distributed Multimedia Systems and Telecommunication Services. Springer; 1997. p. 1–10.
[31] Ren, Y., Cai, T., Tang, M., Wang, L.. AMR steganalysis based on the probability of same pulse position. IEEE Transactions on Information Forensics and Security 2015;PP(99):1–11.
[32] Ren, Y., Yang, J., Wang, J., Wang, L.. AMR steganalysis based on second-order difference of pitch delay. IEEE Transactions on Information Forensics and Security 2017;12(6):1345–1357.
[33] Rugis, J., Klette, R.. A scale invariant surface curvature estimator. In: Advances in Image and Video Technology. Springer; 2006. p. 138–147.
[34] Rusinkiewicz, S.. Estimating curvatures and their derivatives on triangle meshes. In: 3D Data Processing, Visualization and Transmission, 2004. 3DPVT 2004. Proceedings. 2nd International Symposium on. IEEE; 2004. p. 486–493.
[35] Sun, J., Ovsjanikov, M., Guibas, L.. A concise and provably informative multi-scale signature based on heat diffusion. In: Computer graphics forum. Wiley Online Library; volume 28; 2009. p. 1383–1392.
[36] Tang, W., Li, H., Luo, W., Huang, J.. Adaptive steganalysis based on embedding probabilities of pixels. IEEE Transactions on Information Forensics and Security 2016;11(4):734–745.
[37] Tasdemir, K., Kurugollu, F., Sezer, S.. Spatio-temporal rich model-based video steganalysis on cross sections of motion vector planes. IEEE Transactions on Image Processing 2016;25(7):3316–3328.
[38] Taubin, G.. A signal processing approach to fair surface design. In: Proc. of the 22nd annual Conf. on Computer Graphics and Interactive Techniques. ACM; 1995. p. 351–358.
[39] Wang, J., Yang, J., Yu, K., Lv, F., Huang, T., Gong, Y.. Locality-constrained linear coding for image classification. In: Computer Vision and Pattern Recognition (CVPR), 2010 IEEE Conference on. IEEE; 2010. p. 3360–3367.
[40] Wang, K., Lavoué, G., Denis, F., Baskurt, A.. Hierarchical watermarking of semiregular meshes based on wavelet transform. IEEE Transactions on Information Forensics and Security 2008;3(4):620–634.
[41] Wang, K., Torkhani, F., Montanvert, A.. A fast roughness-based approach to the assessment of 3d mesh visual quality. Computers & Graphics 2012;36(7):808–818.
[42] Wang, K., Zhao, H., Wang, H.. Video steganalysis against motion vector-based steganography by adding or subtracting one motion vector value. IEEE Transactions on Information Forensics and Security 2014;9(5):741–751.
[43] Yan, D., Wang, R., Yu, X., Zhu, J.. Steganalysis for MP3Stego using differential statistics of quantization step. Digital Signal Processing 2013;23(4):1181–1185.
[44] Yang, Y., Ivrissimtzis, I.. Polygonal mesh watermarking using Laplacian coordinates. Computer Graphics Forum 2010;29(5):1585–1593.
[45] Yang, Y., Ivrissimtzis, I.. Mesh discriminative features for 3D steganalysis. ACM Transactions on Multimedia Computing,

Communications, and Applications 2014;10(3):27:1–27:13.
[46] Yang, Y., Pintus, R., Rushmeier, H., Ivrissimtzis, I.. A steganalytic algorithm for 3D polygonal meshes. In: Proc. of IEEE Int. Conf. on Image Processing. 2014. p. 4782–4786.
[47] Yang, Y., Pintus, R., Rushmeier, H., Ivrissimtzis, I.. A 3D steganalytic algorithm and steganalysis-resistant watermarking. IEEE Transactions on Visualization and Computer Graphics 2017;23(2):1002–1013.
[48] Yu, J., Li, F., Cheng, H., Zhang, X.. Spatial steganalysis using contrast of residuals. IEEE Signal Processing Letters 2016;23(7):989–992.
[49] Yu, J., Rui, Y., Tao, D.. Click prediction for web image reranking using multimodal sparse coding. IEEE Transactions on Image Processing 2014;23(5):2019–2032.
[50] Yu, J., Yang, X., Gao, F., Tao, D.. Deep multimodal distance metric learning using click constraints for image ranking. IEEE transactions on cybernetics 2016;.
[51] Zhou, W., Yu, L., Qiu, W., Zhou, Y., Wu, M.. Local gradient patterns (lgp): An effective local-statistical-feature extraction scheme for no-reference image quality assessment. Information Sciences 2017;397:1–14.